UAV-Based Hyperspectral Ultraviolet-Visible Interpolated Reflectance Images for Remote Sensing of Leaf Area Index

Tomasz Berezowski ⓘ, *Member, IEEE*, Marcin Kulawiak ⓘ, and Marek Kulawiak ⓘ

Abstract—**Despite its relation to a number of environmental parameters, ultraviolet (UV) reflectance is rarely used in remote sensing. In this study, we investigate the applicability of UV-vis reflectance for vegetation monitoring with unmanned aerial vehicles (UAV). We measure point reflectance over the study area using a UAV-borne spectrometer, project the points onto the Earth's surface, and interpolate them to obtain continuous reflectance images. We use the leaf area index (LAI) to demonstrate the applicability of UV reflectance for vegetation monitoring. Our results show that the UAV reflectance images match the Sentinel-2 reflectance. Our validation shows that the inclusion of UV reflectance to the visible reflectance in LAI models leads to the r^2 increase of up to 29.2% and RMSE decrease of up to 18.9% in comparison to the LAI models using visible reflectance only. We have shown that measurement of UV reflectance is feasible in the 320–400 nm range using UAV remote sensing and that hyperspectral UV-vis reflectance imaging is useful for vegetation monitoring. Moreover, the obtained results lead us to believe that improvement of our measurement system, or conducting the experiments in a different location should make it possible to measure the reflectance at a wavelength of 290 nm. Finally, we discuss other potential applications of UV in remote sensing.**

Index Terms—**Interpolation, hyperspectral imaging, ultraviolet sources, vegetation, vegetation mapping.**

I. Introduction

MONITORING of ultraviolet (UV) reflectance is an important aspect of environmental surveillance, which has gained a lot of attention as advanced spectrophotometers have enabled both laboratory as well as in-situ measurements of the interaction of the UV spectrum with the Earth's flora and fauna. While the entire range of UV radiation is measured in wavelengths from 10 to 400 nm, the portion that reaches the Earth's surface (and thus, is of greatest interest to researchers) is represented by wavelengths between 280 and 400 nm [1], [2].

The fact that the UV and visible (vis) light spectra have similar properties and can be measured by the same instruments enables analysis of an object's absorbance, transmittance, and reflectance over a broader part of the electromagnetic spectrum. This method of research is commonly referred to as UV-vis spectroscopy [3]. In the last decade, the reflectance of ultraviolet and visible wavelengths has been broadly applied to the analysis of water organic and mineral constituents in a variety of cases [4]. Aquatic applications of UV-vis spectroscopy involve the research of marine pollution, both with heavy metals [5] as well as microplastic compounds [6]. Environmental applications of UV-vis also include the detection of atmospheric pollution with various particles, including nitrogen oxide compounds [7], or heavy metals and particulate matter [8]. Ultraviolet spectroscopy is also widely used in monitoring the composition of the atmosphere, including measurement of aerosols' vertical distributions [9] and the identification of explosive compound traces in the atmosphere [10], [11]. An emerging application of UV-vis spectroscopy is the detection of arctic mammals on snow backgrounds [12].

This being said, the prime area of use for ultraviolet reflectance has traditionally been the monitoring of vegetation. Healthy plant leaves have been shown to exhibit increased reflectance in the 280–330 nm wavelength range, and the effect appears to be related to terrain altitude, sun exposition, and season [13], [14]. Other research has shown that narrow-band UV reflectance is correlated with the chlorophyll [15], nitrogen [16], [17], phenolic acid [18], and anthocyanin flavonoids [19] content. Moreover, recent studies suggest that the change in UV reflectance of plant leaves in response to stressors is distinct enough to allow the automated detection of such events within days from infection, even before the occurrence of visual indicators [20].

It needs to be noted, however, that the majority of the aforementioned analyses have been performed either in-situ or in laboratory conditions. Due to atmospheric attenuation, the satellite remote sensing of ultraviolet reflectance is challenging enough to have sparked research on its estimation from visible bands [21], as well as from atmospheric backscattering via a radiative transfer model [22]. The obtained results, due to their limited granularity, are primarily applied to large-scale objects such as algae blooms [23].

In parallel to in-situ and satellite-based observations, there have been several attempts at integrating a UV-capable spectrometer with an unmanned aerial vehicle (UAV) platform. A compact UV spectrometer on a UAV was used for measuring sulfur dioxide atmospheric flux after a volcanic eruption [24].

The spectrometer was designed to observe wavelengths between 245 and 400 nm for the purpose of detecting SO_2 spectral signatures in the air column above the UAV. This application of UV spectroscopy has since become a practice in monitoring volcanic eruptions [25], [26]. Different research has shown that a well-calibrated UAV-based spectrometer can produce reliable point measurements of reflectance below the UAV in the 338–824 nm range at 10-m altitude over land [27]. This being said, the research focused on comparing airborne spectrometer readings to in-situ observations, and did not explore any potential applications of airborne spectroscopy or produce any reflectance images. Another study presented a method of fusing data from an airborne multispectral camera with compact spectrometer footprints for the purpose of obtaining high-resolution imagery for precision farming [28]. However, while the applied spectrometer could measure wavelengths in the range of 350 to 800 nm, the multispectral camera only observed wavelengths of 490 nm, 550 nm, 680 nm, 720 nm, 800 nm, and 900 nm, and thus the proposed methodology was not tested for the UV spectrum. Another approach consisted of a compact spectrometer attached to a UAV for the purpose of monitoring water quality [29]. While that study primarily analyzed spectrometer footprints in nadir in the visible and near-infrared parts of the electromagnetic spectrum (400–800 nm), it also did not produce any reflectance images.

Other UAV-borne spectrometer applications have been applied to land cover classification [30], measuring land surface albedo for hydrological purposes [31], extracting plant phenotype traits [32], and mapping soil organic carbon content [33]; however, none of those use cases involved measurements of the UV spectrum.

While UV-vis spectroscopy has a wide range of applications for in-situ measurements, and certain attempts have been made at its application to satellite and UAV remote sensing, it has not been deeply explored in practical cases. In particular, no applications of UAV-based UV-vis spectroscopy for plant monitoring have been presented, and other uses have been limited to the analysis of point-based measurements in the 350–400 nm range of UV wavelengths. The latter may be partially due to the fact that very few hyperspectral sensors designed for use with drones can measure wavelengths in the UV spectrum, and none of them are sensitive to wavelengths below 350 nm [34].

In this study, we investigate the applicability of UV-vis reflectance for vegetation monitoring using remote sensing. So far, this topic has only been investigated in in-situ laboratory experiments. For this reason, we measure the point reflectance over the study area using a UAV spectrometer, project the points onto the Earth's surface using the UAV's position and orientation, and interpolate them to obtain continuous reflectance images. We validate the images against Sentinel 2 broadband reflectance images. Finally, we demonstrate the applicability of our UV-vis images for leaf area index (LAI) modeling. We use LAI as a proxy for vegetation monitoring because it is easily measured in the field and it correlates with similar visible and infrared spectral features of other vegetation properties such as pigment and nitrogen content [35], [36]. With these experiments, we want to show that the measurement of hyperspectral UV-vis
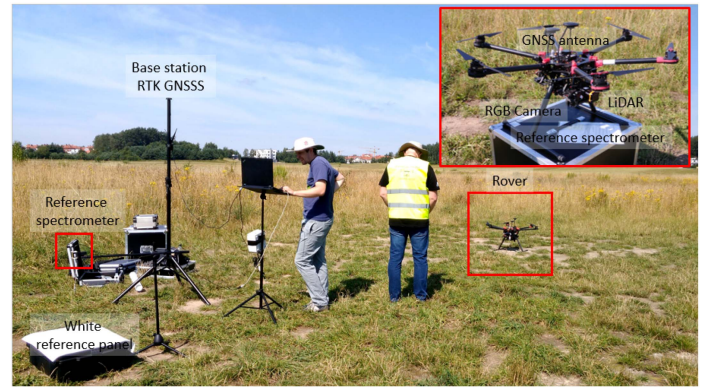

Fig. 1. Measurement system in our study site.

TABLE I
ELLIPTICAL FOOTPRINT OF ROVER SPECTROMETER FOR FLIGHT ALTITUDES USED IN THIS STUDY

Flight altitude [m]	Semi-major axis [m]	Semi-minor axis [m]	Area [m^2]
20	0.35	0.20	0.22
30	0.52	0.30	0.50
60	1.05	0.60	1.98
90	1.57	0.90	4.46

reflectance is feasible using UAV remote sensing and that the reflectance is useful for vegetation monitoring, which has thus far been overlooked in research.

II. METHODS

A. Reflectance Measurements

1) Measurements System: We measured the reflectance factor (hereinafter referred to as "reflectance") using a pair of spectrometers, one of which (rover) was mounted on a UAV platform while the other (reference) was located on the ground (Fig. 1). Both spectrometers were OceanOptics STS UV-VIS with a 189–667 nm overlapping range at an average spectral sampling distance of 0.47 nm. The spectrometers have a 200 μm entrance slit which produces a full width at a half maximum (FWHM) resolution of 12 nm. The radiance was recorded as a digital number (DN) ranging from 0 to 16383 (14 b).

The rover spectrometer was fixed 0.20 m below the GNSS antenna of the UAV and was pointing nadir. The fore optics was a 74-UV-VIS lens to achieve a narrow field of view (FOV). The FOV of this setup, according to our measurements, can be approximated by a 2.00°(in the UAV azimuth direction) by 1.15° ellipse. The on-ground footprint increased with the flight altitude (Table I). The rover spectrometer was controlled by a Raspberry Pi 3 computer, which continuously recorded the radiance data along with the global positioning system (GPS) time, geographical coordinates, and orientation of the UAV.

The reference spectrometer was fixed on a stand pointing nadir at a 0.50 m square PTFE white reference panel. The fore optics was a QP600-025-XSR optical fiber of 0.25 m length, 600 μm diameter, and an average relative transmission in the UV-VIS range of 87%. The optical fiber was used to achieve a broad (25°) FOV while preventing pollution inside the spectrometer, which

would be the case if no fore optics was used. The spectrometer was controlled by the OceanView 1.6.7 software installed on a Windows 10 computer for continuous recording of the radiance diffused from the white reference panel. The computer clock was synchronized to GPS time.

We used a DJI 900 UAV with a PixHawk 2.1 Cube Black flight controller and a Here+ RTK GNSS (rover and base station) with a U-blox NEO-M8P processor. In total, we conducted five UAV flights, three on 2019-07-19 at altitudes of 30 m, 60 m, and 90 m, and two on 2019-09-20 at altitudes of 20 m and 90 m. The flights were conducted using automatic flight mode. The flight lines were directed east-west and distanced by 5 m. The UAV velocity was 2 ms^{-1}.

The reference and rover spectrometers used the same integration time, which was between 40 and 100 ms. A shorter integration time (40 ms) was used for measurement on 2019-07-19 and longer integration times (50–100 ms) were used on 2019-09-20 due to the reduced solar irradiance on that day. Given the UAV velocity of 2 ms^{-1}, the measurement footprint was elongated by 0.08 m and 0.20 m in the azimuth direction for the 40 ms and 100 ms integration times, respectively. Data collected from all sensors was integrated and processed in custom-written software to extract the location and spectral content of every measured point.

2) Reflectance Calculation: The radiance recorded by both spectrometers was interpolated linearly to a 0.5-nm spectral resolution. Further, the reference spectrometer radiance was interpolated linearly in time to match the rover spectrometer measurement time. Following this preprocessing step, the reflectance ρ_λ [-] was calculated as

$$\rho_\lambda = \frac{l_{u,\lambda}}{l_{d,\lambda} c_\lambda} \rho_{r,\lambda} \qquad (1)$$

where λ is the wavelength [nm] for which the reflectance is calculated, $l_{u,\lambda}$[DN] is upwelling radiance factor recorded by the rover spectrometer, $l_{d,\lambda}$[DN] is downwelling radiance factor recorded by the reference spectrometer, $\rho_{r,\lambda}$ [-] is the reflectance of the white reference panel, and c_λ[-] is a calibration factor for the reference spectrometer. Calibration of the reference spectrometer using c_λ is required because each spectrometer has different light transmission due to the fore optics; c_λ also accounts for the manufacturing differences of the spectrometers. Thus, c_λ is the ratio between radiance factors [DN] measured at the same time over the white reference panel using the rover ($l_{ur,\lambda}$) and reference ($l_{dr,\lambda}$) spectrometers

$$c_\lambda = \frac{l_{ur,\lambda}}{l_{dr,\lambda}}. \qquad (2)$$

In this study c_λ was calculated before each UAV flight.

3) Calculation of Measurement Coordinates: We calculated the position of a single reflectance measurement for the rover spectrometer in 3-D space, described by coordinates p_x (easting) [m], p_y (northing) [m], and p_z (elevation) [m], as

$$\begin{bmatrix} p_x \\ p_y \\ p_z \end{bmatrix} = \begin{bmatrix} \cos(\alpha) & -\sin(\alpha) & 0 \\ \sin(\alpha) & \cos(\alpha) & 0 \\ 0 & 0 & 1 \end{bmatrix} \times$$

$$\times \begin{bmatrix} \cos(\beta) & 0 & \sin(\beta) \\ 0 & 1 & 0 \\ -\sin(\beta) & 0 & \cos(\beta) \end{bmatrix} \times$$

$$\times \begin{bmatrix} 1 & 0 & 0 \\ 0 & \cos(\gamma) & -\sin(\gamma) \\ 0 & \sin(\gamma) & \cos(\gamma) \end{bmatrix} \mathbf{S} +$$

$$+ \left(\sqrt{(g_z - h_t)^2 + \tan(\beta)^2 + \tan(\gamma)^2} \begin{bmatrix} g_x \\ g_y \\ g_z \end{bmatrix} \right) \qquad (3)$$

where h_t is known terrain elevation [m], g_x, g_y, and g_z are the sensor's horizontal and vertical position obtained from the UAV GNSS [m], $\mathbf{S}$ is a rotation matrix representing the orientation of the sensor within the UAV, and α, β, and γ represent the UAV's orientation [rad] expressed in yaw, pitch, and roll, respectively, as obtained from the UAV flight controller. Before the calculations, the UAV position is transformed from the original WGS-84 (EPSG:4326) coordinate system into a local projected coordinate system, which in our case was EPSG:2180.

4) Reflectance Images: To derive reflectance images for a given band from point measurements, we used the inverse distance weighted (IDW) algorithm. We chose IDW because it is suitable for interpolation of irregularly distributed data by making it possible to calculate a local result irrespective of the number of neighboring data points. Moreover, our preliminary study showed that IDW is suitable for interpolation of spectral reflectance measurements [37]. An IDW interpolation result in a given block (raster cell) is calculated using measurements located closer than a specified distance. Each measurement contribution is weighted proportionally to its distance to the interpolation block with a certain exponent. In this study, we used an exponent of two, maximum distance for measurement selection of 12 m, and the block size (and interpolation grid) was 5×5 m. The interpolation was conducted using the gstat R package [38].

Before conducting the interpolation, we filtered out measurements that have been assessed as low quality. In the first step, we filtered out measurements for which $l_{d,\lambda}$ <90% of the maximum radiance for a given UAV flight. This step removed measurements affected by cloud coverage, including high clouds such as cirrus, which are difficult to spot with the naked eye. In the second step, we removed measurements where the UAV orientation in any of the yaw, pith, or roll axes changed faster than 12.5°s^{-1}. This step filtered out rapid UAV movements during which the measurement footprint would be too wide for interpolation. The 12.5°s^{-1} angular velocity threshold is equivalent to a 0.44 m footprint elongation at a distance of 50 m at a 40-ms integration time.

To evaluate the quality of the IDW-derived reflectance images, we compared them with Sentinel 2 satellite data. Sentinel 2 has the Multispectral Imager (MSI) sensor with 13 spectral bands in the 443–2202 nm range. The Sentinel 2 bands which overlapped with our spectrometers were aerosol (443 nm), blue (493 nm), green (560 nm), and red (664 nm). We, however, did not use the aerosol band due to a too-low spatial resolution (60 m). The three remaining bands were in 10 m spatial resolution.
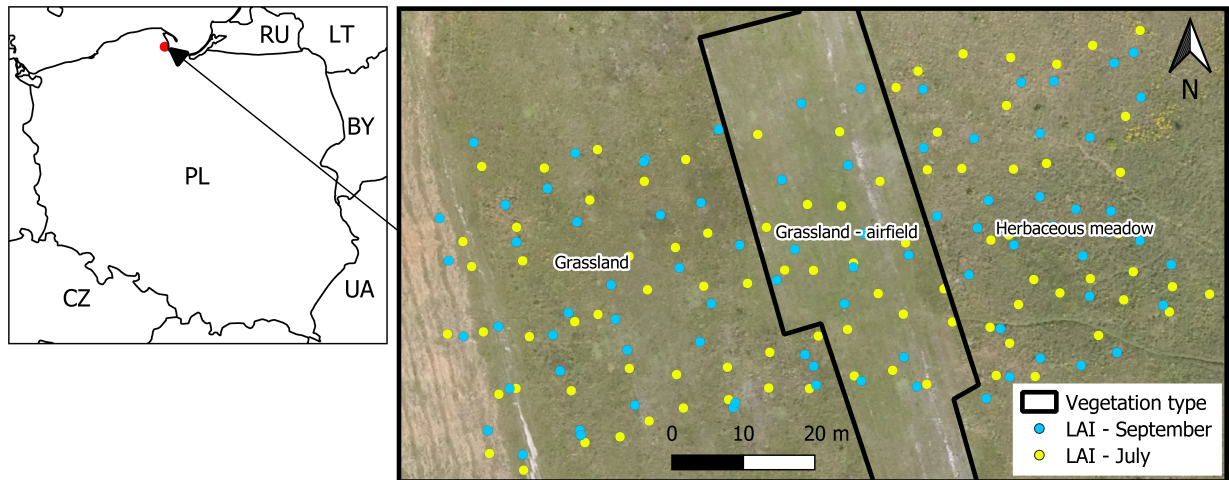
Fig. 2. Study Area with boundary of vegetation types and locations of LAI measurements indicated. A true-color orthoimage acquired on 2019-07-19 is used as the background.

For the comparison, we interpolated the UAV reflectance using IDW to the 10 m raster of the Sentinel 2 image. We used the Sentinel 2 MSI spectral response function to average the UAV reflectance in the Sentinel 2 bands. We performed this validation only for the 2019-07-19 flight at an altitude of 90 m because the reflectance images interpolated for this flight covered the largest area. We did not perform this assessment for the September flights because the Sentinel 2 images acquired close to this time were cloud-covered. We used a Level 2 A Sentinel 2 image acquired on 2019-07-20. The Level 2 A processing produces a bottom-of-atmosphere reflectance orthoimage.

Note that in this validation we used the Sentinel 2 visible bands to validate our method of producing UAV-vis reflectance images. Our reasoning behind this approach was that the Sentinel 2 validation only applies to a part of our methodology workflow, i.e., reflectance sampling using the UAV and interpolation to the images. This is because, for this part of the methodology, the radiative transfer of UV and visible spectrum follows the same principles. To prove that our interpolated UV band images carry valuable information that is different than in the visible band images we performed the LAI modeling and validation (Section II-D).

B. Study Area

Study area was a 6050 m^2 (110×55 m) flat, open area covered by low grassland (57%) and a herbaceous meadow (43%) situated 146 m amsl in the suburbs of Gdynia (18.45° E, 54.50° N), northern Poland (Fig. 2). Within the grassland part, 58% was regularly mowed and used as an amateur airfield; the height of the vegetation was up to 0.15 m with major bare soil gaps. The dominant plant species in the airfield were from the *Poa*, *Pilosella*, and *Aremisia* genera, The remaining 42% of the grassland was occasionally mowed for hay. Within this area, the height of the vegetation was up to 0.35 m and the bare soil gaps were smaller than in the former case. The dominant plant species in the grassland were from the *Poa*,

Aremisia, *Taraxacum*, and *Trifolium* genera. The herbaceous meadow vegetation height was up to 0.80 cm (individual plats reached a height of 1.50 m) and was completely covering the soil. The dominant plant species in the meadow were from the *Poa*, *Rumex*, *Solidago*, *Aremisia*, *Cirisium*, and *Vicia* genera.

The measurements conducted in July reflected vegetation in the second half of the growing season with a number of species blooming. Whereas during the September measurements, the plants were fully developed, with some of the plants in the death phase.

Meteorological data were obtained from the Institute of Meteorology and Water Management in Poland for the Oksywie station located 8.5 km north-east to the study area. During the measurements on 2019-07-19 9:00-12:00 UTC, nearly clear sky conditions were present with cloud cover of 1 to 4 oktas, horizontal visibility of 60 km, wind speed of 5ms^{-1}, and air temperature of 20°C. On 2020-09-20 9:00-12:00 UTC, the cloud cover was 3 to 5 oktas, with horizontal visibility of 60 km, wind speed of 4 ms^{-1}, and air temperature of 14°C.

C. LAI Measurements

We measured the LAI [-] on 2019-07-19 and 2020-09-20 after the last UAV flight conducted for a given day. We used a Li-Cor LAI-2200C device with a view cap that crops the FOV to a 270° quadrant. For each location, we conducted one measurement above the canopy followed by five measurements below the canopy. The below-canopy measurements were distributed within an area of 1 m^2. To minimize the effect of direct sunlight we shaded the sensor during the measurements without affecting the recordings in the 270° FOV. The geographical position of the measurements was recorded by a handheld GNSS device with a horizontal accuracy in open space of less than 2 m [39].

D. LAI Modeling

We used linear regression to model the LAI using reflectance from the UV and visible spectra. Our aim was to test the

applicability of the interpolated UV-vis reflectance images rather than developing a best-possible LAI model. In this case, a linear model highlights better the relationship than a nonlinear machine learning model, which would strongly exploit relations between predictors and would lead to decreased interpretability.

We established separate models for each UAV flight at various spectral resolutions. In each model, the central wavelengths of the bands were the same, i.e. from 340 nm to 620 nm in 40 nm intervals, which resulted in two UV bands and six visible bands. To test the individual potential of the UV and visible bands, we established models in three scenarios: 1) using only the two UV bands; 2) using only the six visible bands; and 3) using all nine UV-vis bands. We obtained the predictors by sampling the reflectance images at the LAI locations without any spatial averaging or buffering. To test the effect of the spectral resolution, we calculated the predictor bands in seven bandwidths: 1 nm, 3 nm, 5 nm, 10 nm, 20 nm, 30 nm, and 40 nm. The widest band was 40 nm because any wider bandwidths would cause band overlapping and inclusion of reflectance below 320 nm (see Section III-A).

We used 50% of the data to train the regression models and the remaining 50% of the sample was used for validation. We quantified the performance of each model by calculating the coefficient of determination r^2 [-] and the root mean squared error (RMSE) [-] between the measured LAI values and the predicted LAI from the validation sample. The r^2 expresses (in the form of a fractional value between 0 and 1) how well the observed LAI variance is replicated by the model. Therefore r^2 shows how each model overall was suitable to explain the relation between the interpolated reflectance images and LAI rather than focusing on the absolute error of the model. The absolute error in the same units as the LAI measurements (dimensionless) was quantified using RMSE, which has the minimum (lowest error) equal to 0.

To identify the importance of predictors in the LAI regression model, we calculated the value of the t statistic [-]. The t statistic is the ratio of the predictor coefficient estimate to the standard error of the coefficient estimate in a linear regression model. The higher the absolute value of the t statistic, the lower the contribution of standard error, hence, the higher the importance of the predictor. Using the t-student statistical distribution, the p-value, or the significance level, was calculated for each t. A p-value smaller than 0.1 or 0.05 usually indicates a significant predictor in a linear regression model.

III. RESULTS

A. Reflectance Measurements

The spread of the reflectance measurement positions and the fraction of the points removed by filtering increased with the rise of the flight altitude (Fig. 3). The applied filtering removed 274 (22%), 278 (28%), and 316 (31%) measurements from the flights at 30, 60, and 90 m, respectively, in July, and 196 (27%) and 187 (31%) measurements from the flights at 20 m and 90 m, respectively, in September. The majority of the removed points were located at the ends of the flight lines, where the UAV had to turn around before measuring the next line.
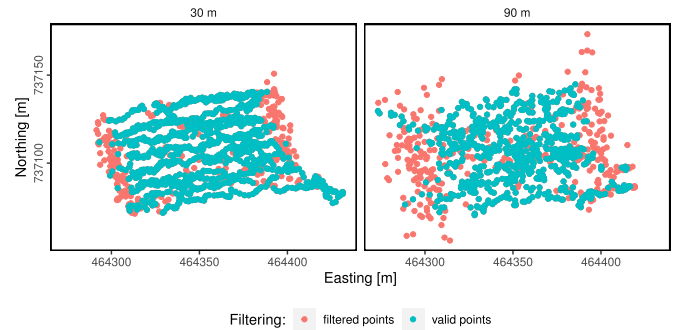

Fig. 3. Reflectance measurements point locations calculated using (3) for 30 m (left) and 90 m (right) flights in July with indication of point locations removed due to filtering.
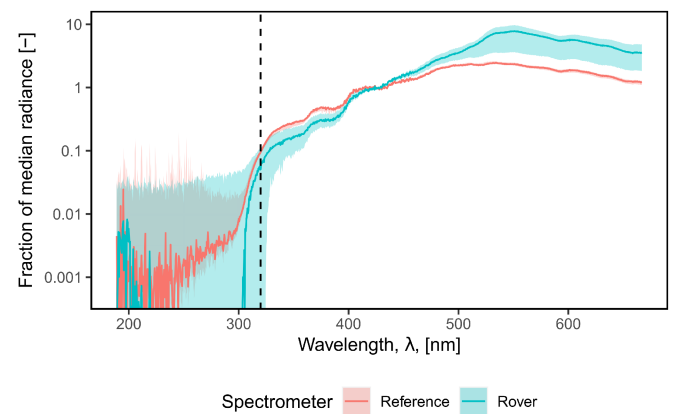

Fig. 4. Median (lines) and 2.5%–97.5% range (polygons) of the radiance factor measurements ($l_{u,\lambda}$ and $l_{d,\lambda}$) normalized to the median of each measurement. The vertical dashed line indicates the 320 nm wavelength threshold above which we used the radiance factor for experiments in this study.

The UV 320–400 nm band radiance was between 9.5% and 70% of the median radiance measured by the reference spectrometer, and between 5.1% and 58 % for the rover spectrometer (Fig. 4). The lowest values occurred for the shortest wavelengths, during the increasing cloud cover in the study area, and over low-UV-reflecting objects (in case of the rover spectrometer). The median DNs for the radiance factor measured by the roving spectrometer, $l_{u,320-400nm}$, were 134 for the 30 m, 166 for the 60 m, and 180 for the 90 m flights in July, and 31 for the 30 m, as well as 73 for the 90 m flights in September. On average, an increase of $l_{u,320-400nm}$ by 1 DN resulted in an increase of $\rho_{320-400nm}$ (1) by 0.0001 and by 0.0007 for the July and September flights, respectively.

The reflectance spectra had a similar shape for different vegetation types in both the July and September measurements (Fig. 5). Higher reflectance in the UV spectrum was denoted for the September than for the July flights. The herbaceous meadow vegetation was characterized by a broader reflectance range in the $\lambda > 600$ nm bands when compared to grasslands for both July and September.

The correlation between the reflectance measurements increased with the increasing flight altitude. Its mean value was
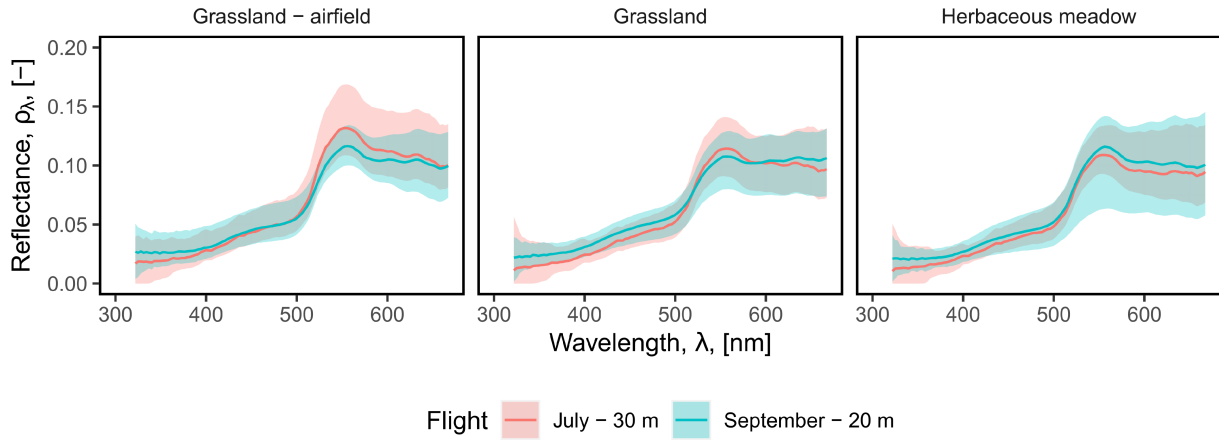
Fig. 5. Median (lines) and 2.5–97.5% range (polygons) of the reflectance (ρ_λ) over three vegetation types present in the study area for July at 30 m and September at 20 m altitude flights.
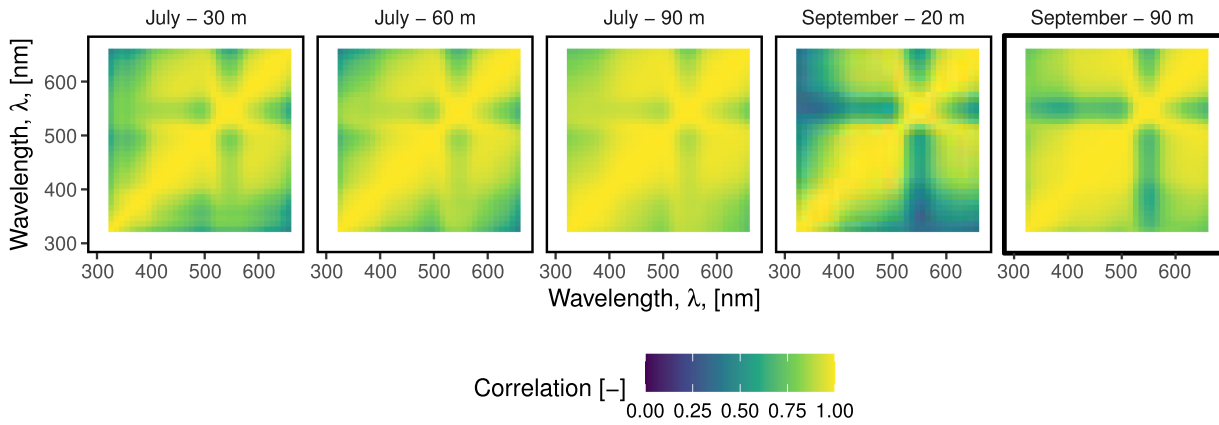

Fig. 6. Correlation between reflectance measurements (ρ_λ) for all flights in July and September.

0.66 (30 m), 0.71 (60 m), and 0.79 (90 m) for the July flights, and 0.64 (20 m), and 0.79 (90 m) for the September flights (Fig. 6). The reflectance was strongly correlated within the visible bands (0.91 mean) except for the 520–570 nm band (0.68 mean). The reflectance was also strongly correlated within the UV bands (0.96 mean). However, a weaker correlation was observed between the UV and visible reflectance, with mean values of 0.77 (30 m), 0.81 (60 m), and 0.88 (90 m) for the July flights, and 0.62 (20 m), and 0.85 (90 m) for the September flights. With the exclusion of the 520–570 nm band, the mean correlation of the UV and visible reflectance was 0.76 (30 m), 0.80 (60 m), and 0.87 (90 m) for the July flights, and 0.66 (20 m), and 0.88 (90 m) for the September flights.

1) Reflectance Images: The smoothness of reflectance images increased with the increase in flight altitude [Fig. 7(a)], but the images acquired on the same day present a similar spatial pattern. Comparison of the images from both dates reveals changes in the vegetation such as a darkening of certain vegetation patches and the removal of bright mowing residues in the western part of the study area. Both UV bands show increased reflectance in September in the south-eastern part of the herbaceous meadow and in the western part of the grassland

[Fig. 7(b)]. The UV reflectance in the airfield remained at a similar level in the images from both dates. Overall, the pattern of UV bands in all captured images is similar, but more details can be noticed in the low-altitude flights.

The blue, green, and red reflectance images matched the Sentinel 2 reflectance [Fig. 8(a)]. Overall, the UAV reflectance overestimated the Sentinel 2 reflectance with the strongest bias in the green band (0.043), followed by the red band (0.040), and the blue band (0.020). The spatial comparison of the reflectance images shows that the shapes of the vegetation features in the UAV datasets resemble those depicted by Sentinel 2 [Fig. 8(b)]. That being said, differences between both images could be distinguished at the boundary.

B. LAI Measurements

In total we sampled 90 and 80 LAI measurements on 2019-07-19 and 2020-09-20, respectively. For the July measurements LAI ranged from 0.05 to 5.22 with a median of 1.36, whereas for the September measurements LAI ranged from 0.00 to 7.39 with a median of 0.81. The LAI median in the herbaceous meadow were the highest of all vegetation types and increased from
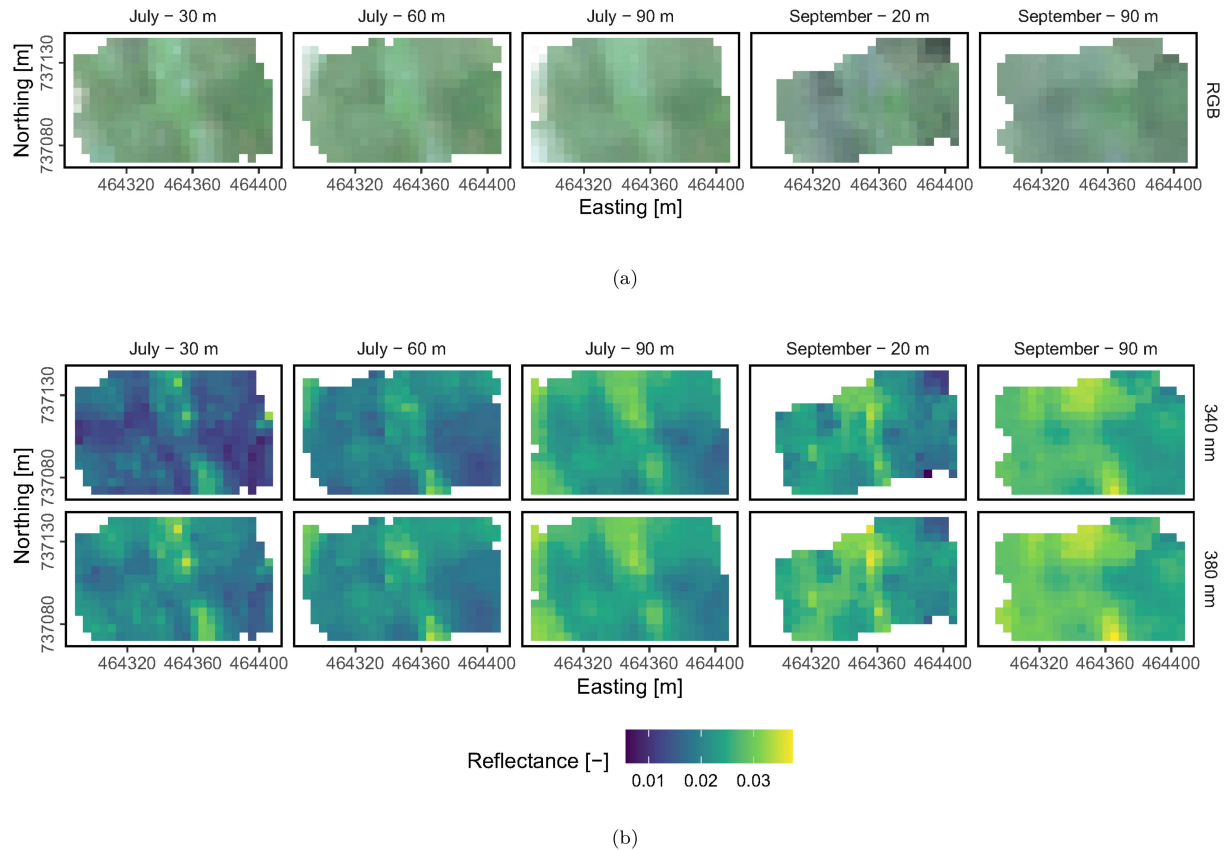
Fig. 7. True-color compositions (a) and the UV reflectance. (b) in 5 nm spectral resolution and 5 m spatial resolution for all UAV flights conducted in this study.

2.77 in July to 3.89 in September. In the mowed grassland the LAI median decreased over time from 1.09 in July to 0.62 in September. Similarly, the LAI median in the airfield decreased from 0.24 in July to 0.08 in September. The highest values of LAI were present in the south-eastern part of herbaceous meadow, where the dense vegetation cover was present, and were equal to 5.52 in July and 7.39 in September.

The measured LAI values were negatively correlated to UV and visible reflectance (Fig. 9). The strongest correlation was for the 520–530 nm bands for the July flights, 450 nm band for the September flight at 20 m, and 375 nm band for the September flight at 90 m. The correlation was stronger for certain UV bands than for such visible bands as $\lambda > 625$ nm, $\lambda \in (400$ nm, 425 nm), or $\lambda \in (490$ nm, 500 nm) for all flights. A weak correlation spectral feature was present in the $\lambda \in (520$ nm, 570 nm) bands in September flight.

C. LAI Modeling

The validation r^2 and RMSE of the LAI regression model depended on the flight altitude, flight period, and the spectral resolution of predictor bands (Fig. 10). The highest r^2 and lowest RMSE for each flight was always achieved for the UV-vis models. Within the July flights, the highest $r^2 = 0.65$ was for the 60 m altitude and 30 nm spectral resolution and the RMSE was 0.767 (15% of the LAI range), whereas for the September flights, the highest $r^2 = 0.69$ was for the 90 m altitude and 20 nm spectral

resolution and the RMSE was 1.20 (16% of the LAI range). The predicted LAI maps show good spatial agreement with the LAI measurement points (Fig. 11).

The inclusion of the UV predictors in the UV-vis models increased the r^2 and decreased the RMSE in reference to the visible predictors models more for the July than for September flights. For the best UV-Vis models, the r^2 increase in reference to the visible predictors models was 9.2% (30 m), 29.2% (60 m), and 10.4% (90 m) for the July flights, and 4.1% (20 m), and 1.2% (90 m) for the September flights. Whereas for the UV-Vis models with the lowest RMSE, the RMSE decrease in reference to the visible predictors models was 3.6% (30 m), 18.9% (60 m), and 6.1% (90 m) for the July flights, and 2.9% (20 m), and 1.7% (90 m) for the September flights.

In the July flights, the UV-vis models had a higher r^2 than the visible predictors models for all spectral resolutions. The visible predictors models had a higher r^2 than the UV models, except for the 90 m flight, with the predictor bandwidth lower than 30 nm. In the September flights, the UV-vis models had a higher r^2 than the visible predictor models for bandwidths greater than 20 nm for the 20 m flight, and greater than 10 nm for the 90 m flight. The same pattern of model quality was observed in terms of the RMSE.

The mean r^2 of the UV models in July for the 90 m flight was 0.47, which was higher than for the 30 m (0.37) and 60 m (0.38) flights. The mean RMSE of the UV models for the 90 m flight was 0.95, which was lower than for the 30 m (1.04) and 60 m
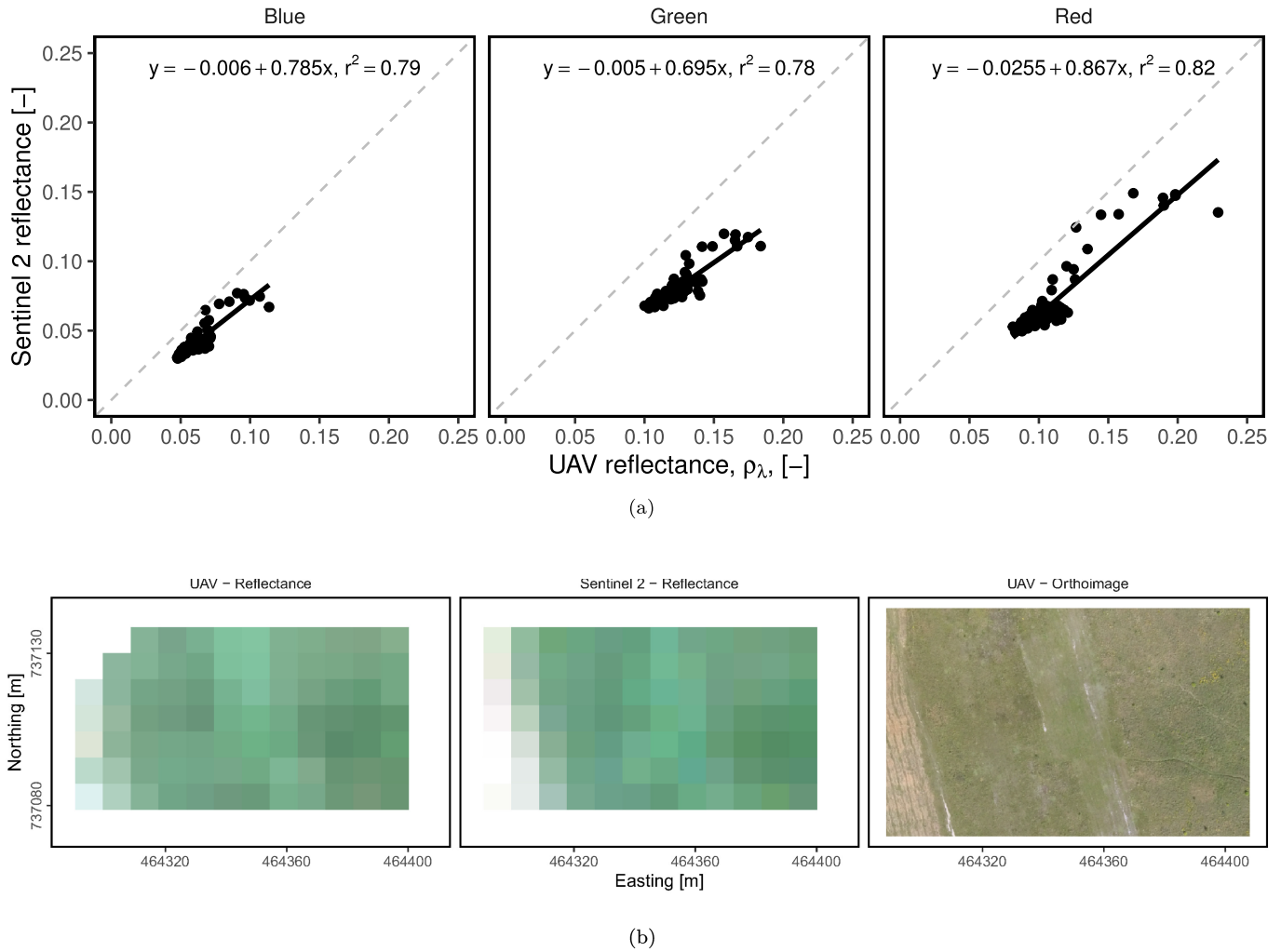
Fig. 8. Comparison of Sentinel 2 reflectance acquired on 2019-07-20 with the UAV reflectance acquired on 2019-07-19 during the 90 m flight. The UAV reflectance was interpolated using IDW to the Sentinel 2 raster (10 m spatial resolution) and averaged using the spectral response function for the Sentinel 2 MSI sensor. The (a) panel presents pixel-by-pixel scatter plots with the 1:1 boundary represented by a dashed gray line. The (b) panel presents a comparison of the RGB images from both sensors, accompanied by a high resolution orthoimage acquired on 2019-07-19 (0.15 m spatial resolution) for reference. Note that the UAV reflectance image has three pixels missing in the NW corner due to a lack of measurement points for interpolation. The UAV orthoimage has a different hue than the reflectance images due to white balance processing by the nonradiometric camera.
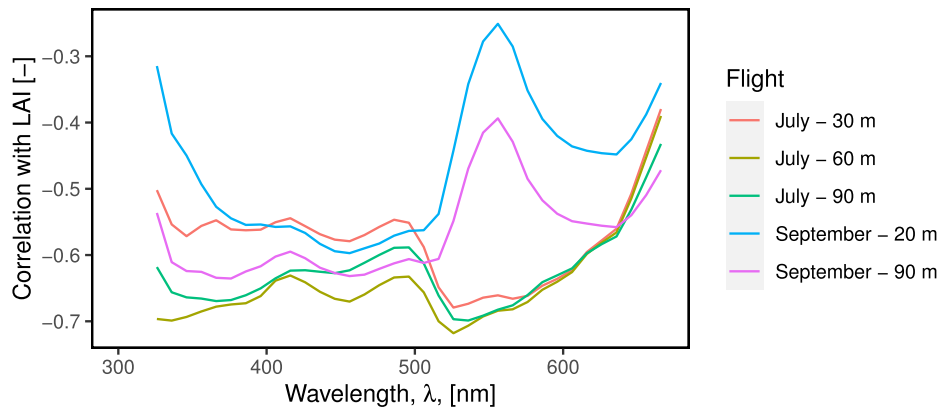

Fig. 9. Correlation coefficient between LAI and reflectance (ρ_λ) for all measurement points.
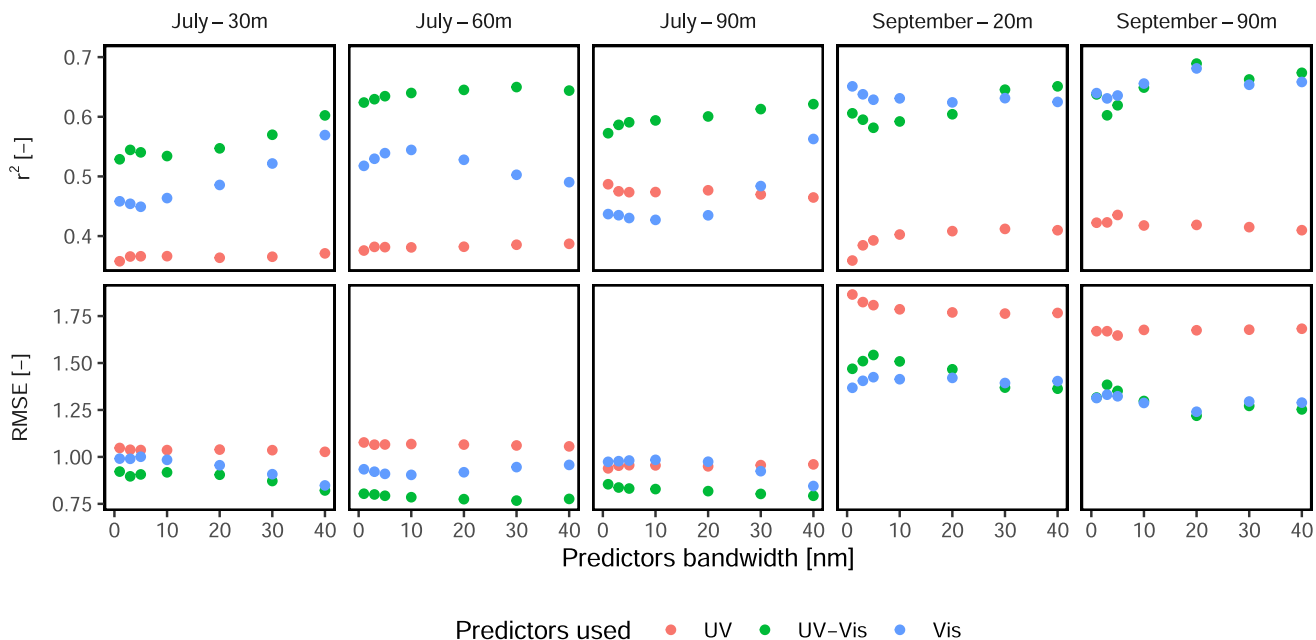
Fig. 10. LAI linear regression models' validation r^2 and RMSE with increasing bandwidth of the predictors for all flights. The values vary by the group of used predictor bands: UV-340 nm, and 380 nm; Vis-420 nm, 460 nm, 500 nm, 540 nm, 580 nm, and 620 nm; UV-vis - all. The RMSE values are in the same units as LAI-dimensionless; the data range of LAI values used for validation was 0.05 to 5.03 in July and 0.00 to 7.39 in September.
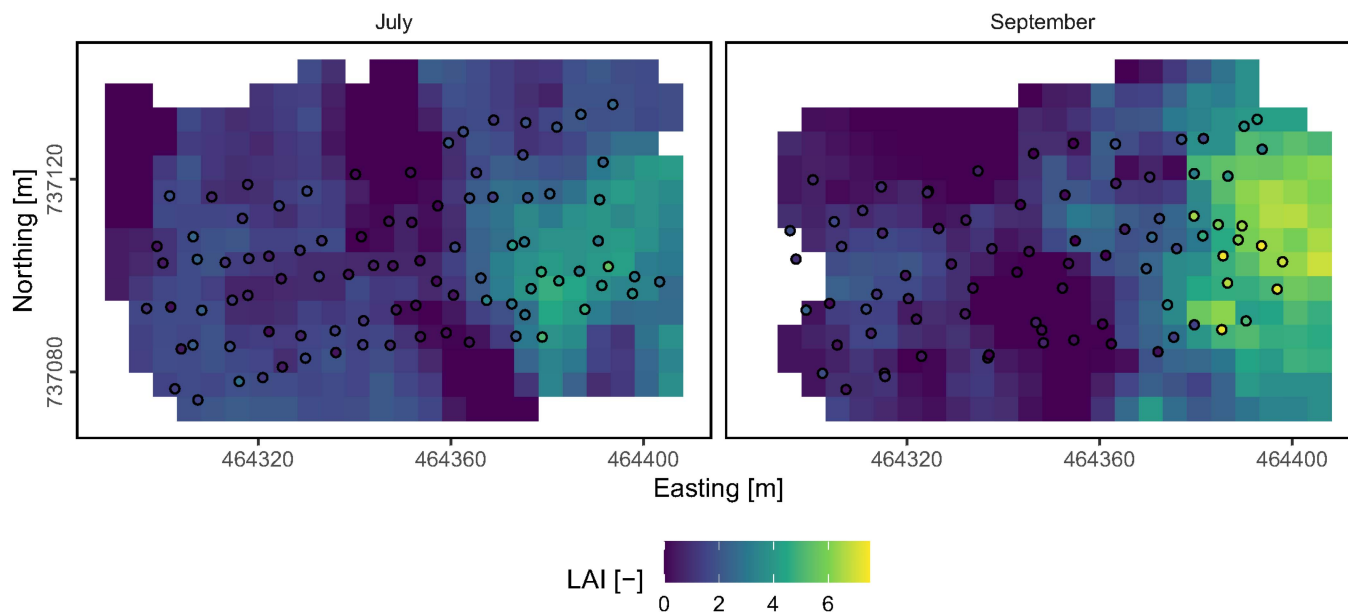

Fig. 11. Predicted LAI maps for the best models from the July (60 m altitude, 30 nm bandwidth) and September (90 m altitude, 20 nm bandwidth) flights. Each map is overlaid by the values of all LAI point measurements sampled on the same day. Color scales are the same for maps and point measurements.

(1.07) flights. The r^2 values for the 90 m flight, unlike for the 30 m and 60 m flights, decreased with the decreasing spectral resolution (the reverse of the increasing bandwidth).

The mean r^2 of the UV models in September was similar for both flights and was equal to 0.40 for the 20 m flight, and 0.42 for the 90 m flight. The r^2 of the UV models clearly decreased for the highest spectral resolution (down to 0.36 for the 1 nm bandwidth) for the 20 m flight. The r^2 of the VIS models decreased for bandwidths greater than 40 nm. The r^2 values in the 90 m flight, unlike in the 20 m flight, decreased with the decreasing spectral
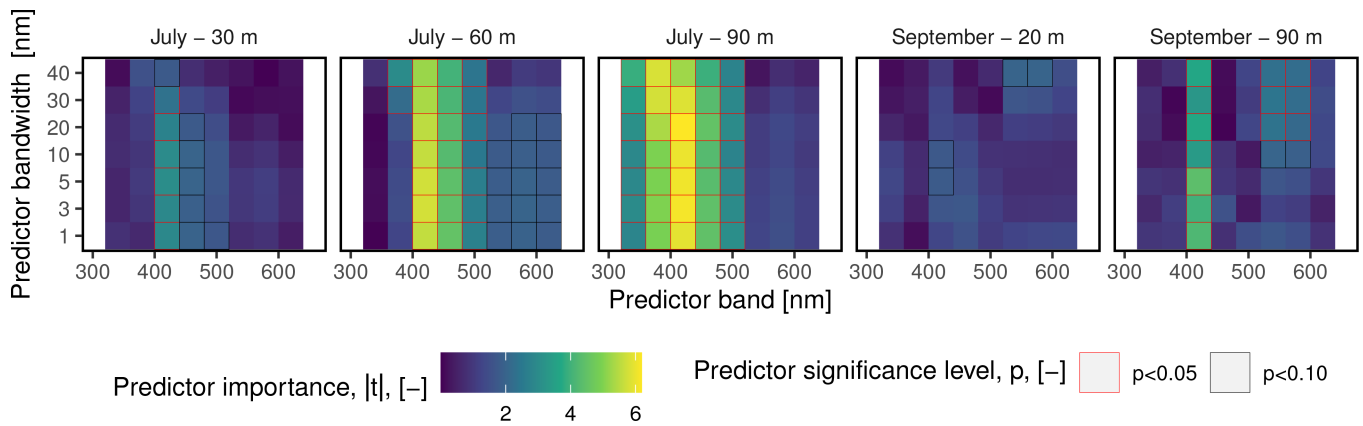
Fig. 12. Importance of the predictor bands as quantified using the t statistics in a linear regression model for UV-Vis models of all flights. Significant predictors are indicated with a red or black frame depending on their significance level (p-value).

resolution. The same pattern of model quality was observed in terms of the RMSE.

The importance of the predictor bands varied with the bandwidth and flight period (Fig. 12). The number of significant predictors increased with the increasing flight altitude for both the June and September flights. The pattern of the predictor importance for the different bandwidths was similar for all altitudes within each month, but varied between the June and September flights. Overall, the most important band was 420 nm, as it was significant in all flights (although not in all bandwidths). The UV predictors were important only in the July flights and their importance was higher for the wider bands. In the September flights this pattern was not observed and none of the UV predictors were significant. Moreover, the 460 nm and 500 nm predictors were not significant in the September flights, unlike in the June flights. The VIS predictor bands with a central wavelength longer than 500 nm were significant only for the July flight at an altitude of 60 m and for both September flights.

Of the UV predictors, the 380 nm band had on average higher importance than the 340 nm band. The 380 nm band was also more often significant, while the 320 nm band was significant only for the June 90 m flight. The 380 nm band was the most important of all predictors in the 40 nm bandwidth model for the July flight at 90 m.

IV. DISCUSSION

A. Reflectance Measurements

The reflectance acquired using the simultaneous measurements of the rover and reference spectrometers showed the expected vegetation pattern in the visible spectrum. When compared to other studies where the UV reflectance for vegetation was measured, the ρ_λ in the UV spectrum was also similar [16], [40]. Initially, we planned to calculate the reflectance with the aid of an atmospheric correction radiative transfer model. However, our simulations with the 6S model [41] indicated that at the flight altitudes up to 90 m and under the atmospheric conditions as in our study, the atmospheric effect on reflectance was negligible. Moreover, [29] have shown that the reflectance in the UV-vis

range for aquatic areas can be measured by a UAV at altitudes of between 20 m and 100 m, given neutral weather conditions.

We were unable to measure the UV reflectance for wavelengths shorter than 320 nm. This limitation was primarily due to the UV reflectance itself, which was as low as 0.02 for the vegetation in the study area. Because of this, the radiance measured by the rover spectrometer for $\lambda < 320$ nm was too low for registration. On the other hand, the reference spectrometer measured radiance DN at a high enough level for wavelengths as short as 290 nm (Fig. 4). The median radiance of the reference spectrometer at $\lambda \in (290\,\text{nm}, 320\,\text{nm})$ was 310 DN, so in an ideal situation, it would be able to measure the reflectance $\rho_{290-320}$ at a resolution of 0.0032. Therefore, if an object with brighter UV reflectance was measured by the rover spectrometer, we would be able to calculate the reflectance for wavelengths shorter than 320 nm. For wavelengths shorter than 290 nm, the solar irradiance (at our geographical latitude and day of the year) was to low to be recorded by the measurement system we used in this study.

The second limitation was the measurement system we used in this study. Radiance measurements at levels higher than the noise in the UV spectrum could theoretically be done if the integration time of the spectrometers was longer. However, practice has shown that a longer integration time than the one used in the presented study would cause elongation of the measurement footprint due to UAV linear and angular velocities. Increasing the integration time could also result in spectrometer saturation for wavelengths with higher solar irradiance than UV or for objects with higher reflectance. A solution to this limitation could be the use of spectrometers with higher sensitivity in the UV spectrum than the silicone CMOS detector used in this study.

The spectrometers we used in this study had a very high spectral sampling resolution (0.47 nm), but lower FWHM (12 nm), which caused averaging of the reflectance from neighboring wavelengths. As a result, we were unable to investigate the effect of narrow UV spectral features for vegetation monitoring as they were attenuated within the FWHM. On the other hand, the effect of deep and narrow spectral features should be, to some extent, visible in the reflectance spectra due to the high spectral

sampling resolution of the spectrometers. This is supported by the fact that the r^2 values were sensitive to the predictor bandwidth in our experiments even for bands narrower than FWHM (Fig. 10). A narrower FWHM could be obtained by using a spectrometer with a narrower slit. On the other hand, a narrower slit decreases the amount of light that enters the spectrometer, increasing the integration time required to achieve the same radiance measurement level. Because the focus of this study was on obtaining UV reflectance at a possibly short wavelength rather than on detecting narrow spectral features, we decided to use a spectrometer with a wide slit.

B. Reflectance Images

Comparison of the UAV reflectance images with the Sentinel 2 reflectance showed that our method of IDW interpolation of projected points of reflectance measurements produces realistic results (Fig. 8). This comparison allowed us to validate the reflectance in the red, green, and blue bands, for which Sentinel 2 provides acceptably high-resolution reflectance data. However, due to the spectrometer's instantaneous measurement of radiance at all wavelengths, we expect that other bands, including UV, were also properly interpolated.

The UAV overestimation of the Sentinel 2 reflectance (Fig. 8) may have at least two sources. The first may be a result of inaccurate measurement of the reference panel for calculating correction factor c_λ ((2)). Any inaccuracy in this step would propagate to all reflectance measurements for which this c_λ was used. Yet, if this was the case, a systematic shift would be observed for the median reflectance between the flights (e.g., in Fig. 5), which did not occur. The second possible source of the reflectance overestimation could be a systematic error in the Sentinel 2 Sen2Cor [42] atmospheric correction method during the Level 2 A product generation. Other studies have also reported overestimation or underestimation of Sentinel 2 Level 2 A products when compared to ground-surface reflectance measurements [43], [44], [45].

While IDW has been shown to produce good-quality reflectance images, other methods, such as linear interpolation (triangulation), or geostatistics could be used instead [37]. The simplest approach would be to use linear interpolation, which is deterministic and does not make any assumptions about the data. However, the linear interpolation approach would not perform well for irregularly distributed data with outliers. In such a case, an outlier could significantly affect the result, as its influence would linearly decrease over a potentially long distance (depending on how sparse are the measurements). On the opposite side, in the case of regular measurements, a linear interpolation approach followed by aggregation to a desired spatial resolution could produce a valid result. Yet, in our case, especially for low-altitude flights, the grid was not regular and locally sparse (between the flight lines). In addition, small footprints were likely to produce outliers (e.g., from small gaps in the vegetation cover). IDW uses information from all neighborhood measurements at a given distance, not only from a given simplex, which attenuates the outliers effect in the interpolated block.

Geostatistical methods such as kriging could also be used instead of IDW. The ordinary kriging interpolation, similarly to IDW, interpolates the result using the neighboring measurements. The difference is that it requires a semivariogram model to be estimated before interpolation for each interpolated variable (each reflectance band in our case). Therefore, ordinary kriging requires more supervision than IDW. Yet, a number of studies have compared ordinary kriging with IDW for different geophysical parameters and shown that they often lead to similar results [46], [47]. Other kriging approaches that could be used for interpolation are co-kriging and kriging with external drift. The co-kriging interpolation uses the relationship with other variables measured at the same locations, but which are unknown elsewhere. In the case of reflectance interpolation, these could be reflectance in other bands. Kriging with external drift uses the relationship with a variable that is known in every location, which could be a multispectral orthoimage acquired using a camera. We are skeptical about both of the latter kriging approaches for reflectance interpolation, because, as we have shown, UV reflectance is not strongly correlated to the reflectance of the visible spectrum (Fig. 6). The use of uncorrelated variables could result in invalid interpolation results, however, this should be investigated in the future.

C. LAI Modeling

Correlation between all bands increases with the increasing flight altitude (i.e., with the increasing spectrometer footprint) due to spatial averaging (Fig. 6). When a gap in the vegetation (e.g., soil, shadow, etc.) covers a high fraction of a spectrometer footprint, the correlation between bands decreases in comparison to a situation where the footprints are larger and each contains a similar fraction of vegetation and gaps. Therefore, an increased spectrometer footprint effectively leads to a more smoothly interpolated reflectance image which lacks spatial features that cause decorrelation between the reflectance in different bands. The low-altitude flights (20 m and 30 m) had too-small footprints, which led to validation with lower r^2 and greater RMSE than for the high-altitude flights from the same day (Fig. 10). At the same time, their lower correlation between the reflectance in the UV and VIS bands (Fig. 6) indicated that the data from the low-altitude flights contained more spectral information.

The UV reflectance was an important predictor for LAI modeling in July (Fig. 10). In particular, the inclusion of UV predictors into the linear regression model resulted in an increased correlation (or decreased scatter) between the measured and modeled LAI in reference to the visual predictors model (Fig. 13). Still, this effect is barely visible for the experiments conducted in September. Another aspect which demonstrates that the UV predictors were irrelevant for the LAI in September is the predictors' importance, which was higher for the July flights (Fig. 12). Also, the correlation of the UV reflectance with the LAI in the September flights decreased in comparison to the flights at similar altitudes (30 m with 20 m, and 90 m with 90 m) in July. Finally, the UV reflectance was less correlated to the visual reflectance in the 60 m and 90 m flights in July than in the September 90 m flight (when excluding the 520–570 nm bands). This means that the UV reflectance in July was related to phenomena that did not affect the visual reflectance, and
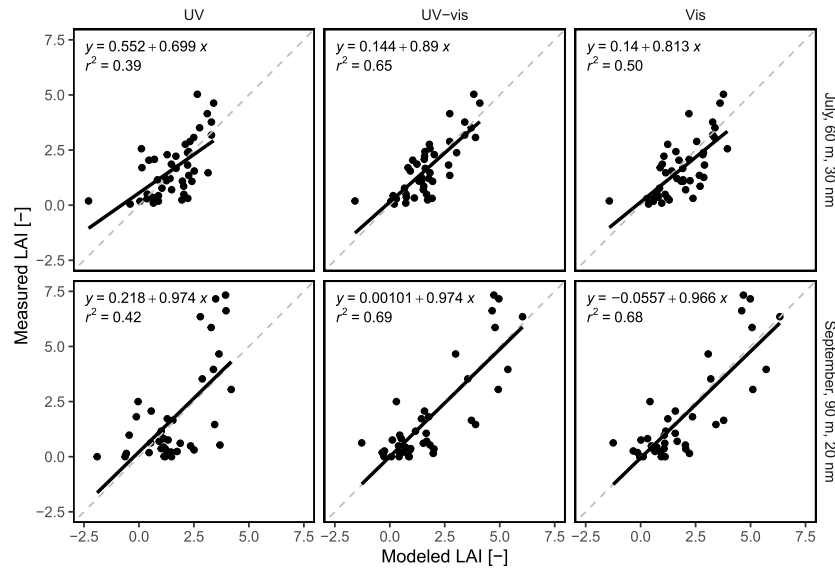
Fig. 13.   Relation between measured and modeled LAI in the validation sample for the models with the highest r^2 in July (60 m altitude, 30 nm spectral resolution) and September (90 m altitude, 20 nm spectral resolution). Panel columns differentiate the plots by the group of predictor bands used in each model.

that did not occur in September. These indicators of decreased modeling applicability of UV bands in September could be related to changes in the vegetation that occurred between the two measurement dates. In September, the LAI values reached their maximum in the herbaceous meadow, whereas they started to decline in the grasslands. Many species were blooming in July, whereas only residues of flowers were occasionally present in September.

In each flight, the 420 nm band was important for the LAI regression. This was likely because green vegetation had much lower reflectance (0.025) than bare soil (0.071) in this band. Given that higher LAI values lead to a decreased soil fraction in the spectrometer footprint, the 420 nm band was a good indicator of the vegetation fraction in a pixel. The 340 nm and 380 nm UV bands also had higher reflectance for bare soil (0.050 and 0.057, respectively) than for green vegetation (0.013 and 0.017, respectively). Therefore, their role in the regression could be similar to the 420 nm band. The ratio between the green vegetation and bare soil reflectance decreased with longer wavelengths. Therefore, the longer wavelength bands were worse for discriminating the bare soil fraction than the shorter wavelengths bands.

As reported in many studies, annual and perennial vegetation change the composition of their pigments (e.g., chlorophylls, carotenoids, or anthocyanins) during their development stages [48], similarly to deciduous trees during senescence [49]. The chlorophylls and carotenoids content in leaves usually exhibit a decline at the end of the phenological cycle [50], [51]. The anthocyanins content pattern is difficult to generalize, because it is often dependent on environmental conditions [48], [52], [53]. The pigments vary in the location of their absorption features in the UV-vis spectrum. The peak absorbance of chlorophyll-a is at 660 nm and 428 nm, chlorophyll-b at 642 nm and 452 nm, and carotenoids within the 436–475 nm range; chlorophyll-a also exhibits higher UV absorbance than chlorophyll-b and

carotenoids, especially in the 300–350 nm range [54]. The peak absorption of various anthocyanins is in the 565–602 nm range also with high absorbance in the UV, especially in the 200–350 nm range [55]. The plant pigments have increased reflectance in certain parts of the UV-vis spectrum: 525–550 nm for chlorophylls, >500 nm and <375 nm for carotenoids, and 375–500 nm for anthocyanins [56]. In this study, we observed increased reflectance in the UV bands in September when compared to the June flights for all vegetation types (Fig. 5), which can be interpreted as decreased absorption of UV light by chlorophyll-a and increased UV reflectance by carotenoids and anthocyanins. A similar effect of decreased UV reflectance was observed when comparing oak leaves from different stands that varied in the composition of their pigments [40]. In the same fashion, the reflectance should also increase between July and September for the 642–660 nm range, which was the case in our study for the grassland (not in the airfield) and herbaceous meadow (Fig. 5).

We expected to observe spectral features characteristic of the presence of flowers, such as an increase of UV, blue and yellow reflectance [56], in the July flights followed by their diminishment in September. To investigate this, we compared the reflectance in July and September in individual spectrometer footprints for areas where flowers were abundant in July (e.g., yellow flowers in the north-eastern part of the study area–Fig. 2). Contrary to expectations, we identified the same reflectance pattern in these locations, as described in the previous paragraph concerning the change in the composition of the pigments.

Of the aforementioned vegetation changes that resulted in modeling differences between the two measurements dates, the highest effect can be attributed to the first one, i.e., the higher soil fraction in the spectrometer footprint. This is confirmed by the presence of a weak correlation in the $\lambda \in (520 \text{ nm}, 570 \text{ nm})$

bands in the September flights (Fig. 9). A further analysis of this feature (data not shown) reveals that it is a result of the high soil fractions (or very low LAI) in the airfield part of the study area. Notably, this weak correlation was not present for other vegetation types in September and was present (but in a stronger form due to the higher LAI) in the airfield in July.

It should be noted that the UV predictors became important only after spectral averaging into broader bands, which may have two reasons. First, there could have been too much noise, especially in the 340 nm band, which prevented the narrow UV bands from being useful predictors. Second, it is possible that the important spectral features for LAI estimation (Fig. 9) did not coincide with the bandwidth intervals selected for this study (every 40 nm), which meant that they were omitted from the narrower bands, but included in the broader bands.

D. Significance of UV Reflectance for Remote Sensing of Vegetation

In our opinion, remotely sensed UV reflectance is an interesting data source that could deliver complimentary information to the currently used near-infrared reflectance. This is because a number of laboratory studies have shown that UV spectral features can be useful for monitoring various aspects of vegetation.

We chose LAI as a proxy for demonstrating the capabilities of UV reflectance for vegetation monitoring because LAI is an easily measurable indicator of vegetation development and vitality. At the same time, however, properties of vegetation such as LAI, pigments content, and nitrogen content not only correlate with the same spectral features in the visible and near-infrared spectrum [35], [36], but often also correlate with one another. Because of this, estimation based on the visible and infrared reflectance makes it hard to distinguish between these individual properties. One solution is the inversion of radiative transfer models, which simulate the effect of the properties of the vegetation on the reflectance [57]. Another solution may be the use of UV reflectance, which has been tested so far in in-situ experiments for vegetation monitoring. The inclusion of UV predictors in vegetation property models other than LAI could be beneficial because UV reflectance can be related to the chlorophyll, nitrogen [15], [16], [17], and phosphorus [58] content in the vegetation. On the other hand, some studies report a weak correlation between the chlorophyll content and UV reflectance [59]. Therefore, such UV reflectance applications still have to be tested in a separate remote sensing field study.

A number of studies have shown that anthocyanins, or more generally flavonoids, in vegetation interact with the UV spectrum by absorbance or reflectance [18], [19], [60], [61]. The presence of these compounds can be used to identify stressed vegetation [62], and their content can also depend on environmental conditions [15]. The fact that parts of the spectrum used in the aforementioned experiments were successfully measured in our study indicates that such measurements could also be performed via UV-vis remote sensing.

Another application of remote sensing in which UV reflectance could be useful is the analysis of plant functional traits. This includes assessment of properties of the leaf epidermis such as pubescence [63] and the presence of wax [64], [65]. However, in such cases, one should proceed with caution as the UV reflectance and transmittance is higher in plants with a thin epidermis than in plants with a thick epidermis, where the UV absorbance is greater [66]. Therefore, the viability of UV remote sensing of the properties of vegetation related to inner leaf cells may be limited in the case of the presence of wax, pubescence, or a thin epidermis.

Moreover, UV reflectance can be useful not only for remotely sensing the properties of an entire canopy, but also for the investigation of smaller objects. The contrast in UV reflectance is used by animals to identify flowers [67]. This feature can be used for improving the remote sensing of pollination type, which thus far has been done with the use of the visible and near-infrared spectrum [68]. UV reflectance is also an early indicator of vegetation disease [20] and therefore could be an interesting alternative to sensing chlorophyll fluorescence in precision agriculture [69]. This being said, the fact that we were unable to identify flowers in our study shows that the remote sensing of such local features is challenging and requires a much higher spatial resolution.

V. Conclusion

In this study, we have demonstrated for the first time a methodology to create hyperspectral UV reflectance (for $\lambda > 320$ nm) images using a low-altitude remote sensing platform and presented its applicability to vegetation monitoring. The UV reflectance obtained in our method was not strongly correlated to the reflectance of visual bands because we interpolated it directly from the measurements. Our technique of producing interpolated reflectance images was accurate, as they resembled very well independent reflectance data from the Sentinel-2 sensor. Our results show that UV reflectance was applicable for vegetation modelling as it was an important predictor that improved LAI modeling in the month of July when compared to models using visual bands only. We attribute this improvement to the sensitivity of UV reflectance to the properties of the vegetation that were pronounced in July. In the month of September, the improvement of LAI modeling by the inclusion of UV reflectance was marginal, which was likely due to the changes in the vegetation properties. Yet, this aspect has to be investigated further in a follow-up study involving measurements of plant pigments. Two very important factors of the presented methodology are the distribution of the reflectance measurement points and their footprint size. In general, small, sparsely distributed footprints have proven to be less valuable for modeling reflectance images than bigger footprints, as the latter provided better spatial averaging.

The obtained results indicate that future research should focus on the following aspects:
1) change of flight parameters and sensors to enable the acquisition of UV reflectance over shorter bands, which in our opinion should be possible down to 290 nm;
2) increase in the density of spectrometer measurement points at low altitudes to obtain an appropriate spatial representation for small footprints;

3) comparison of the UV reflectance with near-infrared reflectance with respect to both information redundancy and the potential for vegetation monitoring;
4) investigation of the feasibility of remotely sensed UV reflectance in the modeling of the properties of vegetation that have thus far been estimated using UV in laboratory analyses.

REFERENCES

[1] J. E. Frederick and D. Lubin, "The budget of biologically active ultraviolet radiation in the earth-atmosphere system," *J. Geophys. Res.*, vol. 93, no. D4, 1988, Art. no. 3825.

[2] S. Madronich, *The Atmosphere and UV-B Radiation at Ground Level*. Boston, MA, USA: Springer, 1993, pp. 1–39.

[3] H. Förster, *UV/VIS Spectroscopy*. Berlin, Germany: Springer, 2004, pp. 337–426.

[4] O. Thomas and C. Burgess, *UV-Visible Spectrophotometry of Water and Wastewater*. Amsterdam, Netherlands: Elsevier, 2017.

[5] Y. Guo, C. Liu, R. Ye, and Q. Duan, "Advances on water quality detection by UV-vis spectroscopy," *Appl. Sci.*, vol. 10, no. 19, 2020, Art. no. 6874.

[6] X.-D. Yang, B. Gong, W. Chen, C. Qian, M. Du, and H.-Q. Yu, "In-situ quantitative monitoring the organic contaminants uptake onto suspended microplastics in aquatic environments," *Water Res.*, vol. 215, 2022, Art. no. 118235.

[7] M. M. Baum, E. S. Kiyomiya, S. Kumar, A. M. Lappas, and H. C. L. III, "Multicomponent remote sensing of vehicle exhaust emissions by dispersive IR and UV spectroscopy," in *Proc. SPIE Infrared Technol. Appl.*, 2000, vol. 4130, pp. 629–639.

[8] S. Galtier, C. Pivard, and P. Rairoux, "Towards DCS in the UV spectral range for remote sensing of atmospheric trace gases," *Remote Sens.*, vol. 12, no. 20, 2020, Art. no. 3444.

[9] L. Wu, O. Hasekamp, B. van Diedenhoven, B. Cairns, J. E. Yorks, and J. Chowdhary, "Passive remote sensing of aerosol layer height using near-UV multiangle polarization measurements," *Geophys. Res. Lett.*, vol. 43, no. 16, pp. 8783–8790, 2016.

[10] D. Mirell, O. Chalus, K. Peterson, and J.-C. Diels, "Remote sensing of explosives using infrared and ultraviolet filaments," *J. Opt. Soc. Amer. B*, vol. 25, no. 7, 2008, Art. no. B108.

[11] T. Ilanko et al., "Ultraviolet camera measurements of passive and explosive (Strombolian) sulphur dioxide emissions at Yasur Volcano, Vanuatu," *Remote Sens.*, vol. 12, no. 17, 2020, Art. no. 2703.

[12] G. Leblanc, C. Francis, R. Soffer, M. Kalacska, and J. de Gea, "Spectral reflectance of polar bear and other large arctic mammal pelts. potential applications to remote sensing surveys," *Remote Sens.*, vol. 8, no. 4, 2016, Art. no. 273.

[13] I. Filella and J. Peñuelas, "Altitudinal differences in UV absorbance, UV reflectance and related morphological traits of quercus ilex and rhododendron Ferrugineum in the mediterranean region," *Plant Ecol.*, vol. 145, no. 1, pp. 157–165, 1999.

[14] J. González, M. Gallardo, C. Boero, M. L. Cruz, and F. Prado, "Altitudinal and seasonal variation of protective and photosynthetic pigments in leaves of the world's highest elevation trees Polylepis tarapacana (Rosaceae)," *Acta Oecologica*, vol. 32, no. 1, pp. 36–41, Jul. 2007.

[15] X. Li, X. Ke, H. Zhou, and Y. Tang, "Contrasting altitudinal patterns of leaf UV reflectance and absorbance in four herbaceous species on the Qinghai-Tibetan plateau," *J. Plant Ecol.*, vol. 12, no. 2, pp. 245–254, 2018.

[16] W. Feng, X. Yao, Y. Zhu, Y. Tian, and W. Cao, "Monitoring leaf nitrogen status with hyperspectral reflectance in wheat," *Eur. J. Agronomy*, vol. 28, no. 3, pp. 394–404, 2008.

[17] S. Rubo and J. Zinkernagel, "Exploring hyperspectral reflectance indices for the estimation of water and nitrogen status of spinach," *Biosyst. Eng.*, vol. 214, pp. 58–71, 2022.

[18] O. Sytar, M. Zivcak, S. Neugart, and M. Brestic, "Assessment of hyperspectral indicators related to the content of phenolic compounds and multispectral fluorescence records in chicory leaves exposed to various light environments," *Plant Physiol. Biochem.*, vol. 154, pp. 429–438, 2020.

[19] V. S. Fedenko, S. A. Shemet, and M. Landi, "UV-vis spectroscopy and colorimetric models for detecting anthocyanin-metal complexes in plants: An overview of in vitro and in vivo techniques," *J. Plant Physiol.*, vol. 212, pp. 13–28, 2017.

[20] A. Brugger, P. Schramowski, S. Paulus, U. Steiner, K. Kersting, and A.-K. Mahlein, "Spectral signatures in the UV range can be combined with secondary plant metabolites by deep learning to characterize barley-powdery mildew interaction," *Plant Pathol.*, vol. 70, no. 7, pp. 1572–1582, 2021.

[21] H. Liu et al., "Estimating ultraviolet reflectance from visible bands in ocean colour remote sensing," *Remote Sens. Environ.*, vol. 258, 2021, Art. no. 112404.

[22] Q. Liu et al., "Deriving surface reflectance from visible/near infrared and ultraviolet satellite observations through the community radiative transfer model," *IEEE J. Sel. Topics Appl. Earth Observ. Remote Sens.*, vol. 15, pp. 2004–2011, 2022.

[23] M. Kahru et al., "Satellite detection of dinoflagellate blooms off California by UV reflectance ratios," *Elementa: Sci. Anthropocene*, vol. 9, no. 1, 2021, Art. no. 00157.

[24] A. J. S. McGonigle, A. Aiuppa, G. Giudice, G. Tamburello, A. J. Hodson, and S. Gurrieri, "Unmanned aerial vehicle measurements of volcanic carbon dioxide fluxes," *Geophys. Res. Lett.*, vol. 35, no. 6, p. L06303, 2008.

[25] T. Mori et al., "Volcanic plume measurements using a UAV for the 2014 Mt. Ontake eruption," *Earth, Planets Space*, vol. 68, no. 1, 2016, Art. no. 49.

[26] J. Rüdiger et al., "Implementation of electrochemical, optical and denuder-based sensors and sampling techniques on UAV for volcanic gas measurements: Examples from Masaya, Turrialba and Stromboli volcanoes," *Atmospheric Meas. Techn.*, vol. 11, no. 4, pp. 2441–2457, 2018.

[27] A. Burkart, S. Cogliati, A. Schickling, and U. Rascher, "A novel UAV-based ultra-light weight spectrometer for field spectroscopy," *IEEE Sensors J.*, vol. 14, no. 1, pp. 62–67, Jan. 2014.

[28] C. Zeng, D. J. King, M. Richardson, and B. Shan, "Fusion of multispectral imagery and spectrometer data in UAV remote sensing," *Remote Sens.*, vol. 9, no. 7, 2017, Art. no. 696.

[29] C. Zeng, M. Richardson, and D. J. King, "The impacts of environmental variables on water reflectance measured using a lightweight unmanned aerial vehicle (UAV)-based spectrometer system," *ISPRS J. Photogrammetry Remote Sens.*, vol. 130, pp. 217–230, 2017.

[30] S. Natesan, C. Armenakis, G. Benari, and R. Lee, "Use of UAV-borne spectrometer for land cover classification," *Drones*, vol. 2, no. 2, 2018, Art. no. 16.

[31] F. Canisius et al., "A UAV-based sensor system for measuring land surface albedo: Tested over a boreal peatland ecosystem," *Drones*, vol. 3, no. 1, 2019, Art. no. 27.

[32] L. Feng, S. Chen, C. Zhang, Y. Zhang, and Y. He, "A comprehensive review on recent applications of unmanned aerial vehicle remote sensing with various sensors for high-throughput plant phenotyping," *Comput. Electron. Agriculture*, vol. 182, 2021, Art. no. 106033.

[33] H. Zhang, P. Shi, G. Crucil, B. Wesemael, Q. Limbourg, and K. V. Oost, "Evaluating the capability of a UAV-borne spectrometer for soil organic carbon mapping in bare croplands," *Land Degradation Develop.*, vol. 32, no. 15, pp. 4375–4389, Aug. 2021.

[34] T. Adão et al., "Hyperspectral imaging: A review on UAV-based sensors, data processing and applications for agriculture and forestry," *Remote Sens.*, vol. 9, no. 11, 2017, Art. no. 1110.

[35] P. Hansen and J. Schjoerring, "Reflectance measurement of canopy biomass and nitrogen status in wheat crops using normalized difference vegetation indices and partial least squares regression," *Remote Sens. Environ.*, vol. 86, no. 4, pp. 542–553, 2003.

[36] S. Jay, F. Maupas, R. Bendoula, and N. Gorretta, "Retrieving LAI, chlorophyll and nitrogen contents in sugar beet crops from multi-angular optical remote sensing: Comparison of vegetation indices and PROSAIL inversion for field phenotyping," *Field Crops Res.*, vol. 210, pp. 33–46, 2017.

[37] T. Berezowski, M. Kulawiak, and M. Kulawiak, "Validation of interpolation algorithms for multiscale UV-VIS imaging using UAV spectrometer," in *Proc. IEEE Int. Geosci. Remote Sens. Symp.*, 2023, pp. 1146–1149.

[38] B. Gräler, E. Pebesma, and G. Heuvelink, "Spatio-temporal interpolation using gstat," *R J.*, vol. 8, no. 1, pp. 204–218, 2016.

[39] Federal Aviation Administration, "Global positioning system standard positioning service performance analysis report," Reporting period, Satellite Navigation Branch, ANG-E66NSTB/WAAS T&E Team, Atlantic City International Airport, NJ 08405, USA, Tech. Rep. 112, Oct.–Dec. 31, 2021.

[40] S. L. Ustin et al., "Retrieval of foliar information about plant pigment systems from high resolution spectroscopy," *Remote Sens. Environ.*, vol. 113, pp. S67–S77, 2009.

[41] S. Y. Kotchenova, E. F. Vermote, R. Matarrese, and F. J. Klemm, "Validation of a vector version of the 6 s radiative transfer code for atmospheric correction of satellite data. Part I: Path radiance," *Appl. Opt.*, vol. 45, no. 26, pp. 6762–6774, 2006.

[42] M. Main-Knorn, B. Pflug, J. Louis, V. Debaecker, U. Müller-Wilm, and F. Gascon, "Sen2Cor for sentinel-2," in *Proc. SPIE Image, Signal Process. Remote Sens.*, 2017, vol. 10427, pp. 37–48.

[43] F. Gascon et al., "Copernicus Sentinel-2 A calibration and products validation status," *Remote Sens.*, vol. 9, no. 6, 2017, Art. no. 584.

[44] O. Hagolle et al., "Sentinel-2 surface reflectance products generated by CNES and DLR: Methods, validation and applications," *ISPRS Ann. Photogrammetry, Remote Sens. Spatial Inf. Sci.*, vol. V-1-2021, pp. 9–15, 2021.

[45] Q.-T. Bui, C. Jamet, V. Vantrepotte, X. Mériaux, A. Cauvin, and M. A. Mograne, "Evaluation of Sentinel-2/MSI atmospheric correction algorithms over two contrasted french coastal waters," *Remote Sens.*, vol. 14, no. 5, 2022, Art. no. 1099.

[46] J. Li and A. D. Heap, "A review of comparative studies of spatial interpolation methods in environmental sciences: Performance and impact factors," *Ecological Inform.*, vol. 6, no. 3/4, pp. 228–241, 2011.

[47] S. Ly, C. Charles, and A. Degré, "Different methods for spatial interpolation of rainfall data for operational hydrology and hydrological modeling at watershed scale: A review," *Biotechnologie, Agronomie, Société et Environnement*, vol. 17, no. 2, pp. 392–406, 2013.

[48] D. A. Sims and J. A. Gamon, "Relationships between leaf pigment content and spectral reflectance across a wide range of species, leaf structures and developmental stages," *Remote Sens. Environ.*, vol. 81, no. 2/3, pp. 337–354, 2002.

[49] L. V. Junker and I. Ensminger, "Relationship between leaf optical properties, chlorophyll fluorescence and pigment changes in senescing Acer saccharum leaves," *Tree Physiol.*, vol. 36, no. 6, pp. 694–711, 2016.

[50] S. Chou et al., "Estimation of leaf photosynthetic capacity from the photochemical reflectance index and leaf pigments," *Ecological Indicators*, vol. 110, 2020, Art. no. 105867.

[51] M. Repajić et al., "Bioactive compounds in Wild Nettle (Urtica dioica L.) leaves and stalks: Polyphenols and pigments upon seasonal and habitat variations," *Foods*, vol. 10, no. 1, 2021, Art. no. 190.

[52] D. C. Close and C. L. Beadle, "The ecophysiology of foliar anthocyanin," *Botanical Rev.*, vol. 69, no. 2, pp. 149–161, 2003.

[53] J. K. Boldt, "Foliar anthocyanins in coleus and ornamental grasses: Accumulation, localization, and function," Ph.D. dissertation, Graduate School, Univ. of Minnesota, Minneapolis, MN, USA, 2013.

[54] H. Lightenthaler, "Chlorophylls and carotenoids: Pigments of photosynthetic biomembranes," *Methods enzymol.*, vol. 148, pp. 350–382, 1987.

[55] K. Yoshida, M. Mori, and T. Kondo, "Blue flower color development by anthocyanins: From chemical structure to cell physiology," *Natural Product Rep.*, vol. 26, no. 7, 2009, Art. no. 884.

[56] E. Narbona, J. C. del Valle, M. Arista, M. L. Buide, and P. L. Ortiz, "Major flower pigments originate different colour signals to pollinators," *Front. Ecol. Evol.*, vol. 9, 2021, Art. no. 743850.

[57] C. Daughtry, C. Walthall, M. Kim, E. de Colstoun, and J. McMurtrey, "Estimating corn leaf chlorophyll concentration from leaf and canopy reflectance," *Remote Sens. Environ.*, vol. 74, no. 2, pp. 229–239, 2000.

[58] M. Ansari, K. Young, and M. Nicolas, "Determining wavelenth for nitrogen and phosphorus nutrients through hyperspectral remote sensing in Wheat (Triticum aestivum L.) plant," *Int. J. Bio-Resour. Stress Manage.*, vol. 7, no. 4, pp. 653–662, 2016.

[59] R. Sonobe, H. Yamashita, A. Y. Nofrizal, H. Seki, A. Morita, and T. Ikka, "Use of spectral reflectance from a compact spectrometer to assess chlorophyll content in Zizania Latifolia," *Geocarto Int.*, vol. 37, no. 18, pp. 5363–5375, Apr. 2021.

[60] H. L. Gorton and T. C. Vogelmann, "Effects of epidermal cell shape and pigmentation on optical properties of antirrhinum petals at visible and ultraviolet wavelengths," *Plant Physiol.*, vol. 112, no. 3, pp. 879–888, 1996.

[61] M. N. Merzlyak, A. E. Solovchenko, A. I. Smagin, and A. A. Gitelson, "Apple flavonols during fruit adaptation to solar radiation: Spectral features and technique for non-destructive assessment," *J. Plant Physiol.*, vol. 162, no. 2, pp. 151–160, 2005.

[62] B. Winkel-Shirley, "Biosynthesis of flavonoids and effects of stress," *Curr. Opin. Plant Biol.*, vol. 5, no. 3, pp. 218–223, 2002.

[63] M. G. Holmes and D. R. Keiller, "Effects of pubescence and waxes on the reflectance of leaves in the ultraviolet and photosynthetic wavebands: A comparison of a range of species," *Plant, Cell Environ.*, vol. 25, no. 1, pp. 85–93, 2002.

[64] J. B. Clark and G. R. Lister, "Photosynthetic action spectra of trees: II. the relationship of cuticle structure to the visible and ultraviolet spectral properties of needles from four coniferous species," *Plant Physiol.*, vol. 55, no. 2, pp. 407–13, 1975.

[65] R. H. Grant, G. M. Heisler, W. Gao, and M. Jenks, "Ultraviolet leaf reflectance of common urban trees and the prediction of reflectance from leaf surface characteristics," *Agricultural Forest Meteorol.*, vol. 120, no. 1/4, pp. 127–139, 2003.

[66] H. W. Gausman, R. R. Rodriguez, and D. E. Escobar, "Ultraviolet radiation reflectance, transmittance, and absorptance by plant leaf epidermises," *Agronomy J.*, vol. 67, no. 5, pp. 720–724, 1975.

[67] S. Papiorek et al., "Bees, birds and yellow flowers: Pollinator-dependent convergent evolution of UV patterns," *Plant Biol.*, vol. 18, no. 1, pp. 46–55, 2015.

[68] H. Feilhauer, D. Doktor, S. Schmidtlein, and A. K. Skidmore, "Mapping pollination types with remote sensing," *J. Vegetation Sci.*, vol. 27, no. 5, pp. 999–1011, 2016.

[69] G. H. Mohammed et al., "Remote sensing of solar-induced chlorophyll fluorescence (SIF) in vegetation: 50 years of progress," *Remote Sens. Environ.*, vol. 231, 2019, Art. no. 111177.

Tomasz Berezowski (Member, IEEE) was born in Warsaw, Poland, in 1986. He received the B.S. and M.S. degrees in environmental protection from the Warsaw University of Life Sciences, Warsaw, Poland, in 2010, and the Ph.D. degree in engineering from Vrije Universiteit, Brussel, Belgium, in 2015.

From 2014 to 2017, he was with the Department of Hydrology and Water Resources, Warsaw University of Life Sciences. Since 2017, he has been an Assistant Professor with the Department of Geoinformatics, Gdańsk University of Technology, Gdańsk, Poland. From 2014 to 2015, he was a Visiting Scholar with Flinders University, Bedford Park, SA, Australia. He has authored or coauthored 24 JCR publications. His research interests include applications of remote sensing in hydrology, especially in hydrological modeling.

Marcin Kulawiak was born in Gdańsk, Poland in 1982. He received the M.S. degree in informatics and the Ph.D. degree in algorithms for processing and visualization of critical infrastructure security data as well as simulation and analysis of threats from the Gdańsk University of Technology (GUT), Gdańsk, Poland, in 2006 and 2010, respectively, and the habilitation degree in technical informatics from the Gdansk University of Technology, in 2018.

From 2007 to 2010, he was a Research Assistant and from 2011 to 2018, he has been an Assistant Professor with the Department of Geoinformatics, Faculty of Electronics, Telecommunications and Informatics, Gdańsk University of Technology. From 2011 to 2013, he worked as a R&D Analyst with OPEGIEKA District Survey. Since 2018, he is an Associate Professor with the Department of Geoinformatics, Faculty of Electronics, Telecommunications and Informatics, Gdansk University of Technology. An expert in Geoinformatics, he has played a leading role in several international R&D projects oriented around dynamic data dissemination and analysis via means of GIS. He has many years of experience working with geographic data of nautical, land, and aerial origin. He has authored or coauthored more than fifty journal articles, presentations on international conferences, and monographs. In his research he has cooperated with international scientific consortia as well as private businesses.

Dr. Kulawiak was the recipient of a gold medal at the prestigious Brussels Innova World Exhibition of Inventions for one of his projects, the Voice Maps system for guiding the visually impaired. He is a Member of the Editorial Board of *Frontiers in Earth Science* and *ISPRS International Journal of Geo-Information*.

Marek Kulawiak was born in Gdańsk, Poland, in 1989. He received the B.S. and M.S. degrees in informatics and the Ph.D degree in processing of hydroacoustic and LiDAR data for construction of three-dimensional models of real world objects from the Gdańsk University of Technology, Gdańsk, Poland, in 2012, 2013, and 2019, respectively.

From 2014 to 2019, he was a Research Assistant with the Department of Geoinformatics, Faculty of Electronics, Telecommunications and Informatics, Gdańsk University of Technology. Since 2019, he has been an Assistant Professor. His main research interests include surface reconstruction, point cloud completion, and machine learning.